Hindawi Publishing Corporation
International Journal of Photoenergy
Volume 2011, Article ID 137328, 7 pages
doi:10.1155/2011/137328

Research Article

Characterization and Catalytic Properties of Nano-Sized Au Metal Catalyst on Titanium Containing High Mesoporous Silica (Ti-HMS) Synthesized by Photo-Assisted Deposition and Impregnation Methods

R. M. Mohamed[1,2] and Elham S. Aazam[1]

[1] *Chemistry Department, Faculty of Science, King Abdul Aziz University, P.O. Box 80203, Jeddah 21589, Saudi Arabia*
[2] *Nanostructured Material Division, Advanced Materials Department, Central Metallurgical R&D Institute, Helwan 11421, Cairo, Egypt*

Correspondence should be addressed to R. M. Mohamed, redama123@yahoo.com

Received 6 May 2011; Accepted 8 June 2011

Academic Editor: David Lee Phillips

The photo-assisted deposition (PAD) and impregnation (img) synthesis of nano-sized Au metal on Ti-HMS are reported. The prepared catalysts were characterized by different techniques such as XRD, XAFS, TEM and nitrogen adsorption analysis. Photocatalytic reactivity using Au/Ti-HMS catalysts under visible-light condition on the oxidation of CO with O_2 reaction was evaluated. The results have shown notable photocatalytic activity of PAD-Au/Ti-HMS which was 2.1 and 5.7 times higher than that of img-Au/Ti-HMS and Ti-HMS, respectively.

1. Introduction

Titanium dioxide (TiO_2) is one of the most intensively studied heterogeneous photocatalysis for the photodEgradation of toxic organic pollutants because it is nontoxic, relatively cheap, chemically stable within a wide pH range, and robust under UV light irradiation [1–7].

Recently, the photodEgradation of some organic dyes using TiO_2 under visible light irradiation has been reported. The studies were significant due to both fundamental and practical aspects exploiting unique mechanisms and perspectives rEgarding treatment of dye pollutants under sunlight. However, the application of TiO_2 in photocatalytic reactions has been impeded as a result of the following obstacles. TiO_2 photocatalysis can only absorb UV light due to their band structure, UV light component in sunlight is a relatively small part (ca. 3–5%) of the solar spectrum, and artificial UV light sources are expensive. Moreover, although fine TiO_2 powders with large specific surface area exhibit high photocatalytic activity, an important issue rEgarding their recovery from aqueous suspensions has been taken into consideration [5–9].

In the last few years, it has been pointed out that there is a strong interest in catalysis by gold due to the potential of highly dispersed gold on various supports to exhibit high catalytic activities for a number of reactions, including CO oxidation [10]; alcohol oxidation [11]; olefin epoxidation [12]; selective hydrogenation of unsaturated hydrocarbons, and so forth, In the past decade, supported gold particles have been applied to catalyze many different types of reactions. The literature reflects a consensus that the preparation method and choice of support significantly influence the size and activity of supported gold. Mesoporous silica, which possesses large pore size and high specific surface area, shows excellent performance for the conversion of bulky reactants and has been considered as notable support for gold loading.

Various materials have been examined for supporting nano-gold. Of these, TiO_2 is extremely active, and on this compound, nano-gold can catalyze CO oxidation at very low temperatures and can catalyze the preferential oxidation

of CO in a hydrogen rich stream (PROX) at around room temperature [13]. However, it is well known that gold catalysts are sensitive to the preparation conditions, gold particle size, and the metal—support interaction. The gold particle size has a strong impact on the activity, because the reactivity of gold clusters depends largely on the type of uncoordinated sites exposed, ensemble effects and metal nanoparticles functionality, which can easily change during the reaction [14]. The influence of the catalyst's preparation method, support type, pretreatment conditions, and Au particle size on the catalytic response of gold catalysts in CO oxidation was extensively reviewed by Bond and Bond and Thompson [15]. The gold-based catalysts also display variable catalytic activity, depending on the support [16]. This is because materials such as SiO_2, Al_2O_3 or MgO are considered to be "inert" supports, which do not participate in the reaction mechanism, whereas transition metal oxides such as Fe_2O_3, CeO_2 or TiO_2 are "active" supports in reactions due to their high oxygen storage capacity and well known catalytic and redox properties. Indeed, most investigators agree that highly active gold catalysts can be supported on pure Fe_2O_3, CeO_2 or TiO_2 materials ([17] and references within). Unfortunately, those reducible oxides have low specific area. As a consequence, gold particles supported on pure Fe_2O_3, CeO_2 or TiO_2 are less stable than those supported on mixed oxide supports [18]. Thus, recently, attempts were conducted by supporting gold catalysts on high surface area (ca. 500–1000 $m^2\,g^{-1}$) mesoporous silica materials such as MCM-48, HMS or SBA-15 [19–21]. In order to increase the oxygen mobility, those materials were modified with small amount of reducible metal oxide [22–24]. The chemical modification of mesoporous silica with transition metal oxides led to an increase of the activity of the total CO oxidation reaction, due to an enhancement of the catalyst thermal stability and minimization of Au particle sintering [25]. The positive effect of dispersing TiO_2 over silica on the stability of Au particles was ascribed in the literature to the inhibition, by development of Si-O-Ti linkages, of the anatase formation upon calcination [26, 27]. Similar to the CO oxidation [22–24], the Au/Ti-SBA-15 systems showed an activity enhancement in the CO-PROX reaction compared to the Ti-free Au/SBA-15 [21].

In the present study, we loaded gold onto Ti-HMS by two methods and applied the product Au/Ti-HMS as a photocatlyst to oxidize CO under visible light irradiation.

2. Experimental Section

2.1. Materials. Tetraethylorthosilicate (TEOS), dodecylamine (DDA), titanium isopropoxide, isopropyl alcohol (IPA) were purchased from Acros Organics Co.

2.2. Synthesis of Ti-HMS. Ti-HMS was synthesized as follows: The first solution (A) was prepared by slowly adding HCl to a mixture of DDA (3 g) and water (30 g) while stirring. The second solution (B) was prepared by adding TEOS (11.8 g) to a mixture of Titanium Isopropoxide (1 g) and IPA (18 g) while stirring. This was followed by adding solution (A) to solution (B) and the resulting solution was stirred for further 20 h, the resultant product was filtered. Finally calcination was carried out at 550°C for 5 h.

2.3. Catalyst Preparation. PAD-Au/Ti-HMS (1 wt% of Au metal) was synthesized using the photo-assisted deposition (PAD) route as follows: Au metal was deposited on Ti-HMS with aqueous solution of $HAuCl_4$ under UV-light irradiation.

Img-Au/Ti-HMS was synthesized by incipient wetness imprEgnation route, Au was loaded onto Ti-HMS with an aqueous solution of $HAuCl_4$ (1 wt% of Au metal). The sample was dried at 378 K then followed by H_2-reduction (20 mL min^{-1}) at 673°C for 2 h.

2.4. Characterization Techniques

2.4.1. X-Ray Diffraction (XRD). To identify the crystallographic phases, the powders were characterized by X-ray diffraction (XRD) (Rigaku RINT, 2000, CuKα radiation, λ = 0.15406 nm).

2.4.2. UV-Vis Diffuse Reflectance Spectra (DRS UV-Vis). Diffuse reflectance ultraviolet-visible absorption spectra (DRS UV-vis) were collected in the UV-vis range (200–800 nm) with $BaSO_4$ as reference on a Shimadzu UV-2450 spectrophotometer at 295 K.

2.4.3. EXAFS. The extended X-ray absorption fine structure (EXAFS) spectra were measured at the BL-7C facility of the Photon Factory at the National Laboratory for High-Energy Physics, Tsukuba. An Si (111) double crystal was used to monochromatize the X-rays from the 2.5 GeV electron storage ring. The Ni K-edge absorption spectrum was recorded in the fluorescence mode at 298 K. The normalized spectra were obtained by a known literature procedure [28], and Fourier transforms were performed on k^3-weighted EXAFS oscillations in the range of 3–10 $Å^{-1}$. The morphologies and particle sizes of the prepared samples were examined with a transmission electron microscope (Hitachi H-9500 operated at 300 kv).

2.4.4. N_2-Adsorption-Desorption Isotherms. The textural properties of the samples were evaluated from the adsorption-desorption isotherms of nitrogen at −196°C detected using a Nova2000 series apparatus (Chromatech). The specific surface areas of the materials were calculated using the BET method within a 0.005–0.30 range of relative pressure (P/P_0). Prior to detection, the samples were dEgassed under vacuum at 270°C for 5 h.

2.5. Reactor Setup and PCO Experimental Procedure. The photocatalytic oxidations of carbon monoxide (PCO) experiments were carried out using a closed-circulation reactor at ambient temperature and pressure. A stainless steel cell (volume, 21 cm^3) with a quartz window (diameter, 3 cm) for UV or visible transmission was connected to a magnetically driven circulation pump through an external Teflon-tubing.

Table 1: Texture parameters of Ti-HM, img-Au/Ti-HMS and PAD-Au/Ti-HMS.

Sample	S_{BET} (m^2/g)	S_t (m^2/g)	S_{meso} (cm^2/g)	S_{micro} (cm^2/g)	S_{ext} (cm^2/g)	V_p (cm^3/g)	V_{micro} (cm^3/g)	V_{meso} (cm^3/g)	r (Å)
Ti-HMS	602	610	408	200	490	0.400	0.040	0.354	21.59
img-Au/Ti-HMS	643	650	300	210	520	0.426	0.052	0.368	20.48
PAD-Au/Ti-HMS	753	750	380	212	640	0.481	0.049	0.436	18.38

Note: (S_{BET}) BET-surface area, (S_t) surface area derived from V_{1-t} plots, (S_{mic}) surface area of micropores, (S_{mes}) surface area of mesopores, (S_{ext}) external surface area, (V_p) total pore volume, (V_{mic}) pore volume of micropores, (V_{mes}) pore volume of mesopores, (r) mean pore radius.

The total volume of the circulation reactor was 100 cm^3. The gas circulation flow rate was about 100 cm^3 min^{-1} and the residence time in the stainless steel reactor was 13 s per cycle. Gases used were CO (500 ppmv in Ar) and CO (500 ppmv in air) as a CO standard, dry air (99.9995%) and Ar (99.9999%) as a carrier gas. Each gas stream was dried by passing through a silica-gel moisture trap.

PCO experiments were carried out with two different initial concentrations of CO; (30 and 500 ppmv). CO concentrations were adjusted by diluting the standard CO gas with the carrier gas using mass flow controllers. The reactor cell was placed in a wooden box that housed a 150-W mercury lamp. The sample was then irradiated with visible light, which was generated by a 150 W high-pressure mercury lamp and an appropriate cut off filter was placed in front of the reactor to remove part of UV radiation.

The removal of CO and the production of CO_2 were monitored using a gas chromatograph; Shimadzu GCMS-QP 5050A; and a gas-sampling valve. The removal efficiency of CO was calculated by applying the following equation:

$$\%\ \text{Removal efficiency} = \frac{C_\circ - C}{C_\circ} \times 100, \quad (1)$$

where $C_\circ$ is the original CO content and C is the retained CO.

3. Results and Discussion

3.1. Characterization of the Fresh Catalysts

3.1.1. X-Ray Diffraction. The hexagonal arrangements of mesoporous silica (HMS) in all synthesized catalysts were confirmed by the low-angle XRD patterns as shown in Figure 1. The absence of diffraction peaks of either crystalline TiO_2 or AuO are indicative of the retention of the mesoporous structure after the application of either photo-assisted deposition (PAD) or imprEgnation (img) method. Also, no diffraction peaks of Au in the patterns of Au-doped samples were observed. This is probably attributed to the low Au doping content (*ca.* 1%). and may imply that Au particles are well dispersed within the Ti-HMS phase.

3.1.2. Textural Properties. For all the catalysts, the surface parameters of surface area and the data calculated from the t-plot are compiled in Table 1. The N_2 adsorption isotherms (not shown here) for the parent and the Au/Ti-HMS are typical of mesoporous solids (type IV), however, an increase in the adsorption capacity of the Ti-HMS was observed after introducing Au ions. From this table the S_{BET} values follow the following order (parent Ti-HMS < img-Au/Ti-HMS < PAD-Au/Ti-HMS). Furthermore, the total pore volume of Au/Ti-HMS is higher than that of Ti-HMS. The values of S_{BET} and S_t are generally close in most samples indicating the presence of mesopores. The values of S_{mic} are low compared to that of S_{mes} implying that the main surface is mesoporous solid as represented by the isotherm. The surface texture data are correlated with the catalytic activity as will be mentioned later on.

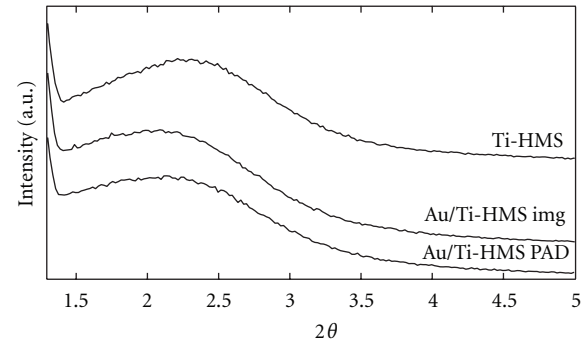

Figure 1: XRD patterns of Ti-HMS (A), PAD-Au/Ti-HMS (B) and img-Au/Ti-HMS (C).

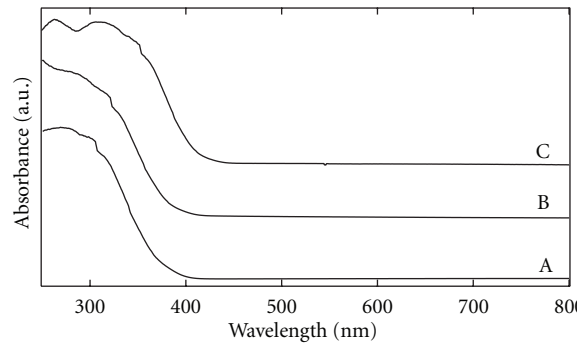

Figure 2: Diffuse reflectance UV-vis absorption spectra of Ti-HMS (A), PAD-Au/Ti-HMS (B) and img-Au/Ti-HMS (C).

3.1.3. UV-Vis Spectroscopy. To gain insight into the effect of Ti/HMS doping with Au, UV-vis diffuse reflectance spectra were recorded at room temperature in the range of 200–900 nm (Figure 2). The Kubelka-Munk function, $F(R)$, can be considered to be proportional to the absorption of radiation [29]. On this basis, the value of E_g , the band gap of the semiconductor, can be derived from the spectra by plotting $(F(R) \cdot h\nu)^{1/2}$ against $h\nu$ as shown in Figure 3 [30].

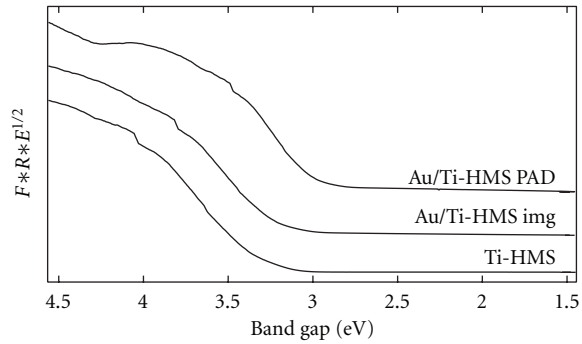

Figure 3: Band-gap calculated from the DR-UV-vis spectra Ti-HMS, img-Au/Ti-HMS and PAD-Au/Ti-HMS.

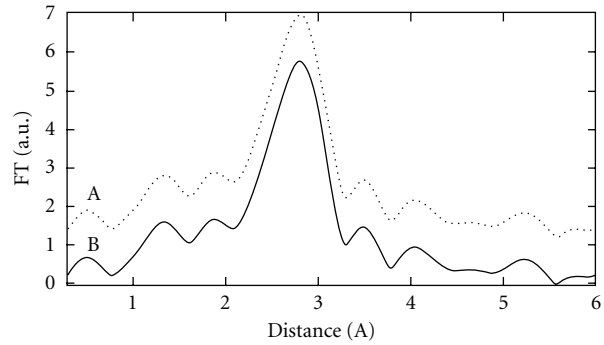

Figure 4: Fourier transforms of the Pt LIII-edge EXAFS spectra for (A) img-Au/Ti-HMS and (B) PAD-Au/Ti-HMS.

Table 2: The calculated band gap energy of Ti-HMS, img-Au/Ti-HMS and PAD-Au/Ti-HMS.

Sample	Baud gap energy (eV)
Ti-HMS	3.2
img-Au/Ti-HMS	3.0
PAD-Au/Ti-HMS	2.7

The E_g values calculated for Ti-HMS, PAD-Au/Ti-HMS and img-Au/Ti-HMS are summarized in Table 2. The band-gap values usually reported for pure anatase and rutile phases are 3.2 and 3.03 eV, respectively [28]. However, these values are influenced by the method of synthesis, the existence of impurities doping the crystalline network and also the average crystal size of the semiconductor.

In a previous study, different methods for calculating E_g values from the UV-vis reflectance spectra were used. For example, some authors calculated the E_g values by a direct extrapolation of the $F(R)$ spectrum whereas others reported the wavelength corresponding to the maximum absorption [31]. As a consequence, quite different E_g values for rutile and anatase samples are found in the literature. For instance, for anatase-based materials, the threshold wavelength values of 370 nm [32], 380 nm [33], 387 nm [34], 393 nm [35] and 403 nm [36] corresponding to a band gap range from 3.08 to 3.35 eV have been reported. In the case of rutile-based materials, an absorption wavelength as high as 437.4 nm ($E_g = 2.84$ eV) has been reported [36].

In the present study, the band gap values calculated for Ti-HMS, img-Au/Ti-HMS and PAD-Au/Ti-HMS are 3.2, 3.0 and 2.7 eV respectively. These data clearly indicate that the study of UV-vis absorption constitutes an important tool for evaluating the changes produced in semiconductor materials by different preparation methods.

3.1.4. EXAFS Measurements. The Fourier transforms of Pt LIII-edge EXAFS spectra of the Au-loaded catalysts are displayed in Figure 4. The presence of the peak at 2.92 Å assigned to the Au-Au bond of Au metal, indicates the formation of nano-sized Au metal [37].

The intensity of the Au-Au peak of the PAD-Au/Ti-HMS catalyst is smaller than the img-Au/Ti-HMS catalyst.

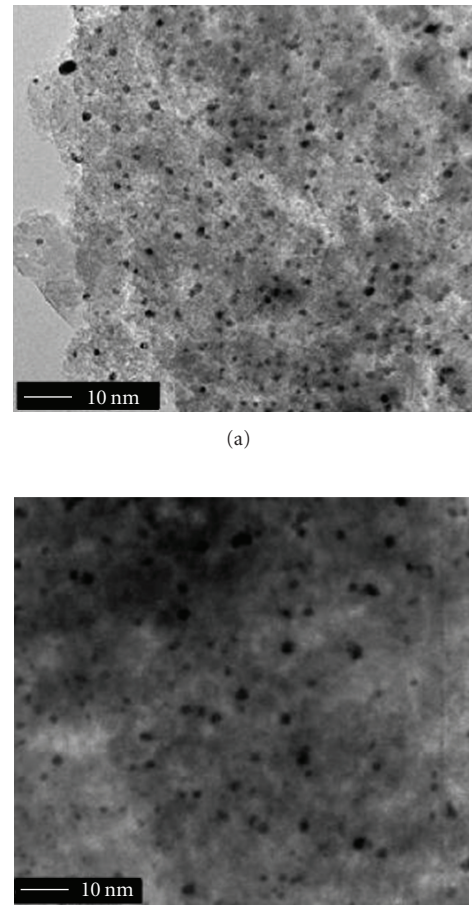

(a)

(b)

Figure 5: The TEM images of the PAD-Au/Ti-HMS (a) and img-Au/Ti-HMS (b) catalyst after H_2 treatment at 473 K.

This relationship clearly suggests that the size of the Au metal particles depends on the preparation method and show smaller particle size formed on the photo-deposited catalyst (PAD-Au/Ti-HMS) than on the img-Au/Ti-HMS catalyst.

3.1.5. TEM Analysis. The TEM images of PAD-Au/Ti-HMS and img-Au/Ti-HMS catalysts are displayed in Figure 5,

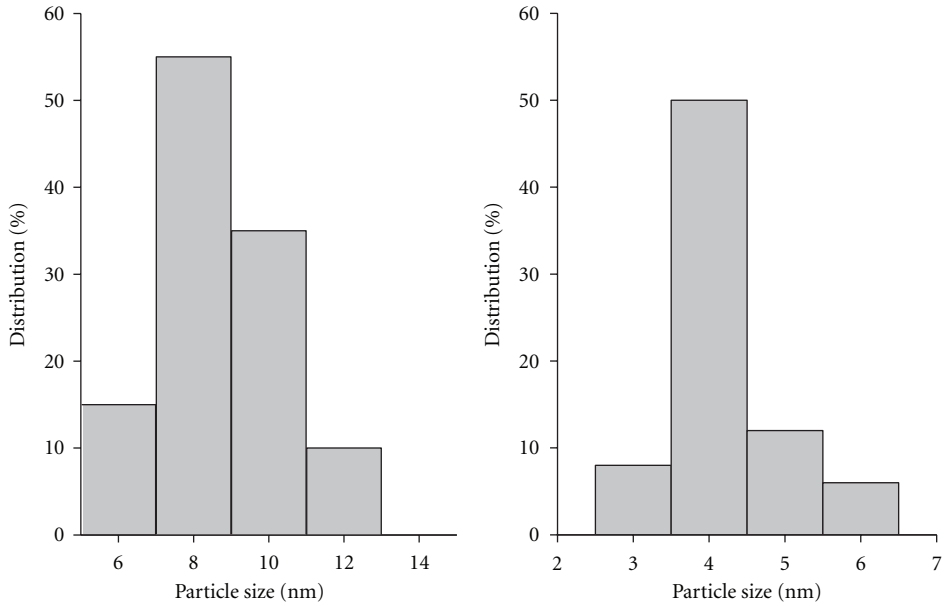

Figure 6: Size distribution diagrams of Au metal obtained from the TEM images of PAD-Au/Ti-HMS (a) and img-Au/Ti-HMS (b) catalyst after H_2 treatment at 473 K.

and the particle distribution obtained from analysis of the TEM images is shown in Figure 6. These data are in strong agreement with the results obtained from EXAFS measurements. Nano-sized Au metal particles having a narrow size distribution (3–6 nm) were found on the PAD-Au/Ti-HMS catalyst, whereas aggrEgated Au metal particles of larger sizes (6–12 nm) were observed on img- Au/Ti-HMS catalyst. These data provide further evidence that the size of the Au metal particles depends on the preparation method.

3.2. Catalyst Testing towards CO Photocatalytic Conversion. The photocatalytic conversion of CO is used as a probe reaction to test the catalytic activity of the prepared nanoparticles. The effect of Ti-HMS, img-Au/Ti-HMS and PAD-Au/Ti-HMS on photocatalytic oxidation of CO at room temperature after 1 h are shown in Figure 7. The data demonstrate that the photocatalytic activities of the PAD-Au/Ti-HMS (97.8%) are higher than that of img-Au/Ti-HMS (47.9%) and the parent Ti-HMS (17.1%). Considering that, the pure Au oxides don not have photocatalytic oxidation properties, such variation in activity must be due to the differences in interaction between Au and Ti-HMS that led to several modifications in the physical properties such as band gap, particle size and surface texture. Also, we can observe that, the catalytic activity of Ti-HMS generally increased with the addition of Au promoters. A maximum activity was obtained in the case of PAD-Au/Ti-HMS. The correlation between the photoactivity and the physical properties such as band gap, surface area and pore volume is depicted in Figure 8. It is clear that, the photocatalytic activity was at a maximum in the case of PAD-Au/Ti-HMS

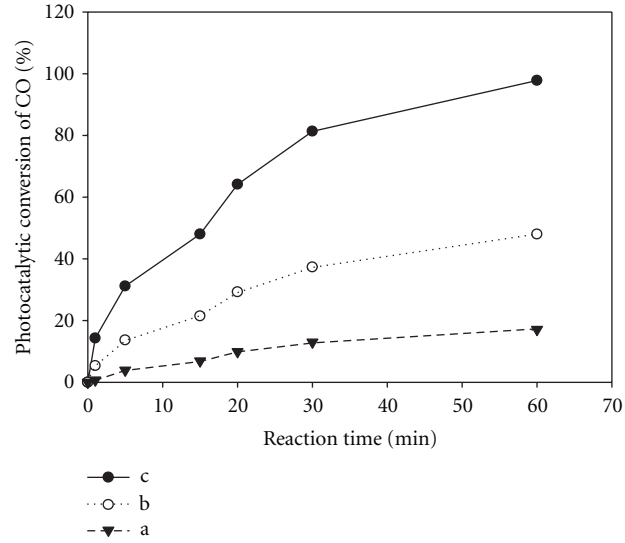

Figure 7: Photocatalytic conversion of CO (%) for Ti-HMS (a), img-Au/Ti-HMS (b) and PAD-Au/Ti-HMS (c).

in which the surface area and pore volume were maximum but band gap was minimum.

In addition, Figure 8 shows the good correlation between the band gap, surface area and pore volume with the catalytic activity where the activity is gradually increasing with the decrease of band gap and the increase of the surface area and pore volume.

It is believed that the lack of electron scavengers (surface Ti^{4+}) and hole traps (surface hydroxyl groups) is responsible for the rapid recombination rate of e^-/h^+, which leads to lower photocatalytic activity. The results show that the

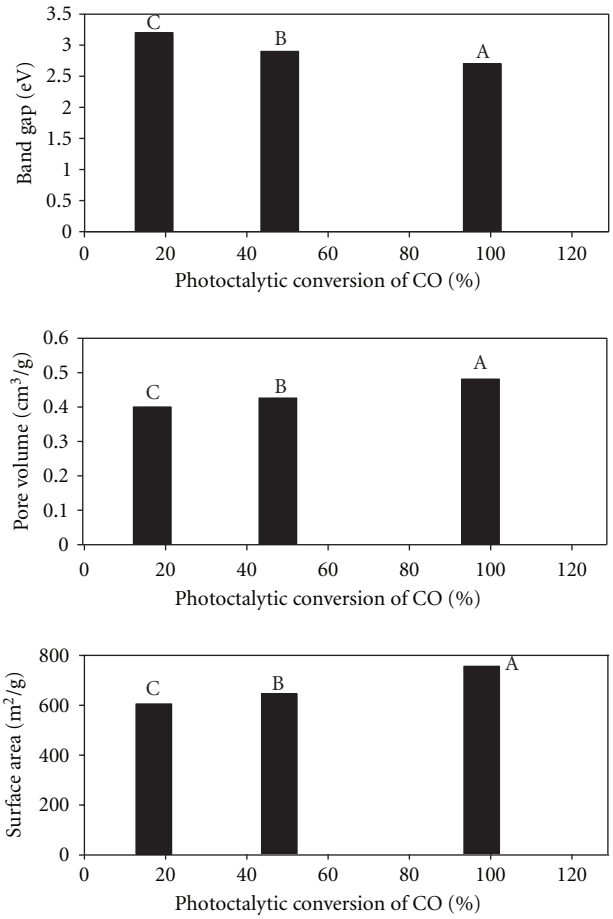

Figure 8: Effect of physical parameters of the materials on their photocatalytic activity for PAD-Au/Ti-HMS (A), img-Au/Ti-HMS (B) and Ti-HMS (C).

photocatalytic activities of the Au/Ti-HMS nanoparticles increased with decreasing the band gap. This is due to the low energy to exit electron from valance band to conduction band. Also, the PAD- Au/Ti-HMS has the best photoactivity, since it has the lowest band gap and particle size and the highest surface area and pore volume.

4. Conclusions

It can be concluded that the nano-sized particles of Au/Ti-HMS can be prepared via two methods: photo-assisted deposition (PAD) and the conventional imprEgnation method (img). The characterization of such prepared catalysts by N_2 adsorption, XRD, UV-vis and EXAFS techniques reveals the following remarks.

(1) The nano-sized Au metal with a mean diameter (d) of ca. 4 nm having a narrow size distribution was found on the PAD-Au/Ti-HMS catalyst, whereas the aggrEgated Au metal with various sizes are observed on img-Au/Ti-HMS catalyst ($d \sim 10$ nm).

(2) The calculated values of band gap for Ti-HMS, img-Au/Ti-HMS and PAD-Au/Ti-HMS are 3.2, 2.9 and 2.7 eV respectively.

(3) The N_2 adsorption isotherms for the parent and the Au/Ti-HMS are typical of mesoporous solids, the surface area changed from 602 to 643 and 753 m^2/g in case of img-Au/Ti-HMS and PAD-Au/Ti-HMS respectively.

(4) The intensity of the Au-Au peak of the PAD-Au/Ti-HMS catalyst is smaller than the img-Au/Ti-HMS catalyst. These findings suggest that the size of Au metal particles depends on the preparation method. Au metal particles formed on the photo-deposited catalyst (PAD-Au/Ti-HMS) show smaller particle sizes than those obtained from the imprEgnated catalyst (img-Au/Ti-HMS).

References

[1] X. Z. Li and F. B. Li, "Study of Au/Au^{3+}-TiO_2 photocatalysts toward visible photooxidation for water and wastewater treatment," *Environmental Science and Technology*, vol. 35, no. 11, pp. 2381–2387, 2001.

[2] R. Zanella, S. Giorgio, C. R. Henry, and C. Louis, "Alternative methods for the preparation of gold nanoparticles supported on TiO_2," *The Journal of Physical Chemistry B*, vol. 106, no. 31, pp. 7634–7642, 2002.

[3] H. Li, Z. Bian, J. Zhu, Y. Huo, H. Li, and Y. Lu, "Mesoporous Au/TiO_2 nanocomposites with enhanced photocatalytic activity," *Journal of the American Chemical Society*, vol. 129, no. 15, pp. 4538–4539, 2007.

[4] V. Subramanian, E. E. Wolf, and P. V. Kamat, "Catalysis with TiO_2/gold nanocomposites. Effect of metal particle size on the Fermi level equilibration," *Journal of the American Chemical Society*, vol. 126, no. 15, pp. 4943–4950, 2004.

[5] J. Li, C. Chen, J. Zhao, H. Zhu, and J. Orthman, "Photodegradation of dye pollutants on TiO_2 nanoparticles dispersed in silicate under UV-VIS irradiation," *Applied Catalysis B*, vol. 37, no. 4, pp. 331–338, 2002.

[6] J. Li, C. Chen, J. Zhao, H. Zhu, and Z. Ding, "Photodegradation of dye pollutants on TiO_2 pillared bentonites under UV light irradiation," *Science in China Series B*, vol. 45, no. 4, pp. 445–448, 2002.

[7] J. Li, W. Ma, C. Chen, J. Zhao, H. Zhu, and X. Gao, "Photodegradation of dye pollutants on one-dimensional TiO_2 nanoparticles under UV and visible irradiation," *Journal of Molecular Catalysis A*, vol. 261, no. 1, pp. 131–138, 2007.

[8] C. Chen, X. Li, W. Ma, J. Zhao, H. Hidaka, and N. Serpone, "Effect of transition metal ions on the TiO_2-assisted photodegradation of dyes under visible irradiation: a probe for the interfacial electron transfer process and reaction mechanism," *The Journal of Physical Chemistry B*, vol. 106, no. 2, pp. 318–324, 2002.

[9] W. Zhao, C. Chen, X. Li, J. Zhao, H. Hidaka, and N. Serpone, "Photodegradation of sulforhodamine-B dye in platinized titania dispersions under visible light irradiation: influence of platinum as a functional co-catalyst," *The Journal of Physical Chemistry B*, vol. 106, no. 19, pp. 5022–5028, 2002.

[10] M. Haruta, "Size- and support-dependency in the catalysis of gold," *Catalysis Today*, vol. 36, no. 1, pp. 153–166, 1997.

[11] C. H. Christensen, B. Jørgensen, J. Rass-Hansen et al., "Formation of acetic acid by aqueous-phase oxidation of ethanol with air in the presence of a heterogeneous gold catalyst," *Angewandte Chemie—International Edition*, vol. 45, no. 28, pp. 4648–4651, 2006.

[12] M. D. Hughes, Y.-J. Xu, P. Jenkins et al., "Tunable gold catalysts for selective hydrocarbon oxidation under mild conditions," *Nature*, vol. 437, no. 7062, pp. 1132–1135, 2005.

[13] W.-Y. Yu, C.-P. Yang, J.-N. Lin, C.-N. Kuo, and B.-Z. Wan, "Preparation of Au/TiO_2 for catalytic preferential oxidation of CO under a hydrogen rich atmosphere at around room temperature," *Chemical Communications*, no. 3, pp. 354–356, 2005.

[14] L. Barrio, P. Liu, J. A. Rodriguez, J. M. Campos-Martin, and J. L. G. Fierro, "Effects of hydrogen on the reactivity of O_2 toward gold nanoparticles and surfaces," *The Journal of Physical Chemistry C*, vol. 111, no. 51, pp. 19001–19008, 2007.

[15] G. C. Bond and D. T. Thompson, "Catalysis by gold," *Catalysis Reviews—Science and Engineering*, vol. 41, no. 3-4, pp. 319–388, 1999.

[16] E. Quinet, F. Morfin, F. Diehl, P. Avenier, V. Caps, and J.-L. Rousset, "Hydrogen effect on the preferential oxidation of carbon monoxide over alumina-supported gold nanoparticles," *Applied Catalysis B*, vol. 80, no. 3-4, pp. 195–201, 2008.

[17] A. S. K. Hashmi and G. J. Hutchings, "Gold catalysis," *Angewandte Chemie—International Edition*, vol. 45, no. 47, pp. 7896–7936, 2006.

[18] F. Moreau, G. C. Bond, B. van der Linden, B. A. A. Silberova, and M. Makkee, "Gold supported on mixed oxides for the oxidation of carbon monoxide," *Applied Catalysis A*, vol. 347, no. 2, pp. 208–215, 2008.

[19] M. Bandyopadhyay, O. Korsak, M. W. E. van den Berg et al., "Gold nano-particles stabilized in mesoporous MCM-48 as active CO-oxidation catalyst," *Microporous and Mesoporous Materials*, vol. 89, pp. 158–163, 2006.

[20] A. Beck, A. Horváth, G. Stefler et al., "Formation and structure of Au/TiO_2 and Au/CeO_2 nanostructures in mesoporous SBA-15," *Catalysis Today*, vol. 139, no. 3, pp. 180–187, 2008.

[21] M. Ruszel, B. Grzybowska, M. Laniecki, and M. Wójtowski, "Au/Ti-SBA-15 catalysts in CO and preferential (PROX) CO oxidation," *Catalysis Communications*, vol. 8, no. 8, pp. 1284–1286, 2007.

[22] J. A. Hernandez, S. Gómez, B. Pawelec, and T. A. Zepeda, "CO oxidation on Au nanoparticles supported on wormhole HMS material: effect of support modification with CeO_2," *Applied Catalysis B*, vol. 89, no. 1-2, pp. 128–136, 2009.

[23] L. Escamilla-Perea, R. Nava, B. Pawelec, M. G. Rosmaninho, C. L. Peza-Ledesma, and J. L. G. Fierro, "SBA-15-supported gold nanoparticles decorated by CeO_2: structural characteristics and CO oxidation activity," *Applied Catalysis A*, vol. 381, no. 1-2, pp. 42–53, 2010.

[24] C. L. Peza-Ledesma, L. Escamilla-Perea, R. Nava, B. Pawelec, and J. L. G. Fierro, "Supported gold catalysts in SBA-15 modified with TiO_2 for oxidation of carbon monoxide," *Applied Catalysis A*, vol. 375, no. 1, pp. 37–48, 2010.

[25] R. J. H. Grisel and B. E. Nieuwenhuys, "Comparative study of the oxidation of CO and CH_4 over $Au/MO_x/Al_2O_3$ catalysts," *Catalysis Today*, vol. 64, no. 1-2, pp. 69–81, 2001.

[26] G. J. Hutchings, "Catalysis by gold," *Catalysis Today*, vol. 100, no. 1-2, pp. 55–61, 2005.

[27] T. V. Choudhary and D. W. Goodman, "Oxidation catalysis by supported gold nano-clusters," *Topics in Catalysis*, vol. 21, pp. 25–34, 2002.

[28] M. Schiavello, *Heterogeneous Photocatalysis*, Wiley, Chichester, UK, 1997.

[29] M. Anpo and M. Che, "Applications of photoluminescence techniques to the characterization of solid surfaces in relation to adsorption, catalysis, and photocatalysis," in *Advances in Catalysis*, B. C. G. Werner, O. Haag, and K. Helmut, Eds., pp. 119–257, Academic Press, New York, NY, USA, 1999.

[30] G. Lassaletta, A. Fernández, J. P. Espinós, and A. R. González-Elipe, "Spectroscopic characterization of quantum-sized TiO_2 supported on silica: influence of size and TiO_2-SiO_2 interface composition," *The Journal of Physical Chemistry*, vol. 99, no. 5, pp. 1484–1490, 1995.

[31] R. J. Davis and Z. Liu, "Titania-silica: a model binary oxide catalyst system," *Chemistry of Materials*, vol. 9, no. 11, pp. 2311–2324, 1997.

[32] R. M. Mohamed and I. A. Mkhalid, "The effect of rare earth dopants on the structure, surface texture and photocatalytic properties of TiO_2-SiO_2 prepared by sol-gel method," *Journal of Alloys and Compounds*, vol. 501, no. 1-2, pp. 143–147, 2010.

[33] K. Kosuge and P. S. Singh, "Titanium-containing porous silica prepared by a modified sol-gel method," *The Journal of Physical Chemistry B*, vol. 103, no. 18, pp. 3563–3569, 1999.

[34] A. A. Belhekar, S. V. Awate, and R. Anand, "Photocatalytic activity of titania modified mesoporous silica for pollution control," *Catalysis Communications*, vol. 3, no. 10, pp. 453–458, 2002.

[35] B. J. Aronson, C. F. Blanford, and A. Stein, "Solution-phase grafting of titanium dioxide onto the pore surface of mesoporous silicates: synthesis and structural characterization," *Chemistry of Materials*, vol. 9, no. 12, pp. 2842–2851, 1997.

[36] S. Cheng, S.-J. Tsai, and Y.-F. Lee, "Photocatalytic decomposition of phenol over titanium oxide of various structures," *Catalysis Today*, vol. 26, no. 1, pp. 87–96, 1995.

[37] P. R. Sarode, K. R. Priolkar, P. Bera, M. S. Hegde, S. Emura, and R. Kumashiro, "Study of local environment of Ag in Ag/CeO_2 catalyst by EXAFS," *Materials Research Bulletin*, vol. 37, no. 9, pp. 1679–1690, 2002.